JACS
JOURNAL OF THE AMERICAN CHEMICAL SOCIETY

Communication

pubs.acs.org/JACS

Antiphase Dual-Color Correlation in a Reactant–Product Pair Imparts Ultrasensitivity in Reaction-Linked Double-Photoswitching Fluorescence Imaging

Wei Wan,[†] Ming-Qiang Zhu,[‡] Zhiyuan Tian,*[,§] and Alexander D. Q. Li*[,†]

[†]Department of Chemistry and Center for Materials Research, Washington State University, Pullman, Washington 99164, United States

[‡]Wuhan National Laboratory for Optoelectronics, Huazhong University of Science and Technology, Wuhan 430074, P. R. China

[§]School of Chemistry and Chemical Engineering, University of Chinese Academy of Sciences, Beijing 100049, P. R. China

Supporting Information

ABSTRACT: A pair of reversible photochemical reactions correlates their reactant and product specifically, and such a correlation uniquely distinguishes their correlated signal from others that are not linked by this reversible reaction. Here a nanoparticle-shielded fluorophore is photodriven to undergo structural dynamics, alternating between a green-fluorescence state and a red-fluorescence state. As time elapses, the fluorophore can be in either state but not both at the same time. Thus, the red fluorescence is maximized while the green fluorescence is minimized and vice versa. Such an antiphase dual-color (AD) corelationship between the red and green fluorescence maxima as well as between their minima can be exploited to greatly improve the signal-to-noise ratio, thus enhancing the ultimate detection limit. Potential benefits of this correlation include elimination of all interferences originating from single-color dyes and signal amplification of AD photoswitching molecules by orders of magnitude.

Correlation using physical properties has enabled an array of new microscopic technologies.[1] However, correlation linked by chemical reactions has rarely been exploited. Herein we report the gain of ultrasensitivity using a chemical correlation based on a reactant–product pair that interconvert via reversible photochemical reactions.

The photosensitive reactant and product are methoxyspiropyran (MSP) and methoxymerocyanine (MMC) that were covalently polymerized into nanoparticles: MSP emits green fluorescence (λ_{max} = 530 nm), while MMC emits red fluorescence (λ_{max} = 665 nm) (Figure 1A). Because MSP and MMC are linked via two reversible photochemical reactions, their fluorescence properties are also correlated in the same manner. As depicted in Figure 1A, MSP can be photochemically converted to MMC via either a single photon in the UV region (≤420 nm)[2] or two photons in the near-infrared (NIR) region (700–780 nm).[3] Conversely, MMC can be photochemically converted back to MSP under visible-light illumination (500–600 nm), thus completing one reversible cycle (k = 1; N = 1 for MSP and 2 for MMC).

Photoswitching between MSP and MMC yields a spatial resolution of ∼20 nm,[4] but this work focuses on sensitivity gains using the antiphase relationship between the green and red fluorescence maxima (Figure 1B). This correlation is underpinned by the photochemical reactions, which specify that green fluorescence maxima appear at λ = 530 nm and $t = (2k - 1)\pi$ while the red fluorescence is maximized at λ = 665 nm and $t = 2k\pi$. The large difference between the green and red fluorescence maxima (>130 nm) enables easy separation with minimal cross-interference. The photoswitching generates a time delay between the green and red fluorescence, resulting not in a simple on–off relationship[5] but rather in an antiphase relationship where the red fluorescence is maximized at even phase (2π, 4π, 6π, etc.) and the green fluorescence is maximized at odd phase (π, 3π, 5π, etc.).

While the time dimension reveals first-order kinetics of the photochemical reactions, the wavelength dimension depicts the spectral change as a function of the molecular structure. Figure 1C shows the spectral profiles corresponding to the horizontal lines in Figure 1B as the red-emitting nanoparticles in solution were photoswitched to green-fluorescing nanoparticles over a period of 500 s (1.5 nM, 1 cm path length, 450 W Xe lamp through double monochromators, λ = 365 nm).[6] However, it took just ≤0.3 s to photochemically switch MMC to MSP for either single-particle studies or live-cell imaging (vide infra). Therefore, the absolute amount of time required to complete the photoswitching cycle is less meaningful because the solution concentration, optical path length, solution volume, light intensity, reaction rate, and wavelength all contribute to it. A more meaning way to describe time in such photochemical reaction kinetics is to use the periodicity that corresponds to reactant and product cycles. In Figure 1C, the odd phase π indicates the photoswitching molecule has the MSP structure, whereas the even phase 2π corresponds to the MMC structure. The intermediate states at times of $5\pi/4$, $3\pi/2$, and $7\pi/4$ reveal that various amounts of MSP in the nanoparticles have been photochemically switched to MMC or vice versa. As the time finishes a half-period ($t \approx$ 500 s for solution, t = 0.02–0.3 s for imaging), the green emission gradually shifts to red emission, as evidenced in Figure 1C.

To exploit the antiphase relationship between the red and green fluorescence from a single molecule, we designed

Received: January 29, 2015
Published: March 16, 2015

© 2015 American Chemical Society

DOI: 10.1021/jacs.5b01007
J. Am. Chem. Soc. 2015, 137, 4312–4315

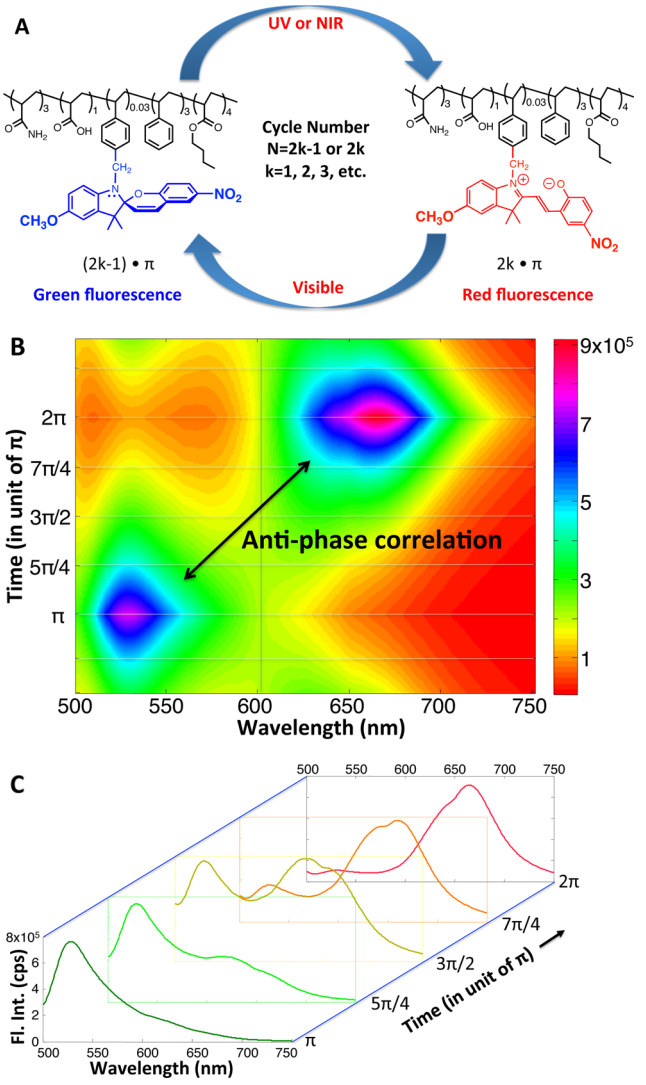

Figure 1. (A) UV or NIR light drives the conversion of green-emitting polymer nanoparticles (PNPs) containing MSP into the red-emitting PNPs containing MMC, and visible light drives the reverse process. (B) Two-dimensional contour plot revealing the AD correlation or half-period of π shift between the green and red maxima. (C) Horizontal cross-section profiles showing the photochemical conversion of green-fluorescing PNPs to red-emitting PNPs over the time period of π.

antiphase dual-color (AD) correlation microscopy (Figure S1 in the Supporting Information (SI)), in which the signal of each cycle is defined as the product of the dual-color fluorescence minima subtracted from the product of the dual-color fluorescence maxima (eq 1):

$$P_{\mathrm{corr}}(i,j) = \sum_{k=1}^{N/2} [P_{\mathrm{green}}(i,j,(2k-1)\pi)P_{\mathrm{red}}(i,j,2k\pi) - P_{\mathrm{green}}(i,j,2k\pi)P_{\mathrm{red}}(i,j,(2k-1)\pi)] \quad (1)$$

where $P_{\mathrm{corr}}(i,j)$ is the pixel intensity of position (i,j) in the AD correlated image. At the same pixel, the green fluorescence maximum $P_{\mathrm{green}}(i,j,(2k-1)\pi)$ and its concomitant red fluorescence minimum $P_{\mathrm{red}}(i,j,(2k-1)\pi)$ occur at odd π, whereas the green fluorescence minimum $P_{\mathrm{green}}(i,j,2k\pi)$ and its concomitant red fluorescence maximum $P_{\mathrm{red}}(i,j,2k\pi)$ occur at even π. The first term, the product of the green and red fluorescence maxima, boosts the correlation signal strength while the second term, the product of the fluorescence minima, removes noise and interference because these minima are mostly noise and interference. For normal constantly emitting fluorophores, these two terms nullify each other. Single-molecule blinking can cause nonperfect cancellation, but shortening the exposure time minimizes this effect. The key point is that AD fluorophores clearly stand out among normal fluorophores.

Figure 2A,B illustrates the green (505−543 nm) and red (610−800 nm) fluorescence images, respectively, with the

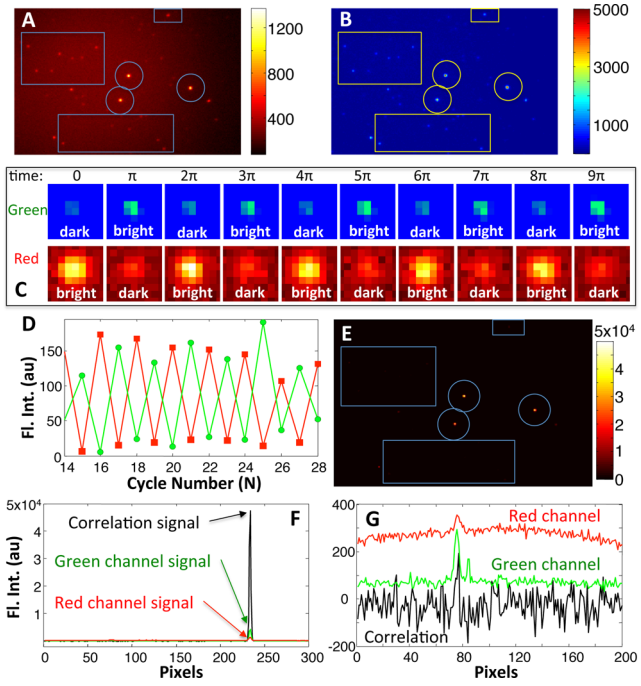

Figure 2. (A, B) Dual-color PNPs were imaged: (A) red and (B) green integrated fluorescence intensities. (C, D) For a single particle, the red and green emissions have a half-period phase shift, with red emission maximized at even frames corresponding to $2k\pi$ and green fluorescence maximized at odd frames corresponding to $(2k-1)\pi$. (E) AD correlation imaging removes those signals that have no such correlation (signals in boxes) and enhance those from AD PNPs (signals in circles). (F, G) Line profiles passing through AD PNPs reveal that the intensities of the correlation signals are orders of magnitude larger than those of the single-channel integrated signals (A or B).

antiphase signals in circles and non-antiphase signals in boxes. Zooming in on a single AD nanoparticle (Figure 2C) reveals that the spot fluoresces green at times corresponding to odd π and emits red fluorescence at times corresponding to even π. The plot of the integrated fluorescence intensities (Figure 2D) confirmed the antiphase relationship. Applying eq 1 to process every individual pixel (i,j), we obtain the AD correlated image in Figure 2E, which exhibits two salient features. First, all of the interfering signals and noise in the boxes disappeared because they were not photoswitching and were removed by the second term in eq 1. Thus, the AD correlation imaging technology is superior at eliminating noise and interference generated by normal dyes.

Second, the alternating dual-color signals are significantly enhanced, as the intensity scale jumps by an order of magnitude. The quantitative enhancement created by AD

DOI: 10.1021/jacs.5b01007
J. Am. Chem. Soc. 2015, 137, 4312−4315

correlation is presented in Figure 2F,G. The signal-to-noise (S/N) ratios in the green and red channels at a circled spot are 132 and 43.3, respectively. However, the S/N ratio in the AD correlation is improved to 825, which is higher than those of the green and red channels by factors of 6.25 and 19, respectively. Similar S/N enhancements of 3.47- and 3.52-fold over the green channel and 14.7- and 54.2-fold over the red channel were observed for other circled spots because the even AD noise is about doubled but the AD signals are enhanced by orders of magnitude.

The litmus test for AD correlation imaging is whether such a new technology can deliver superior S/N in live-cell imaging. Figure 3A illustrates the alternating dual-color bright−dark

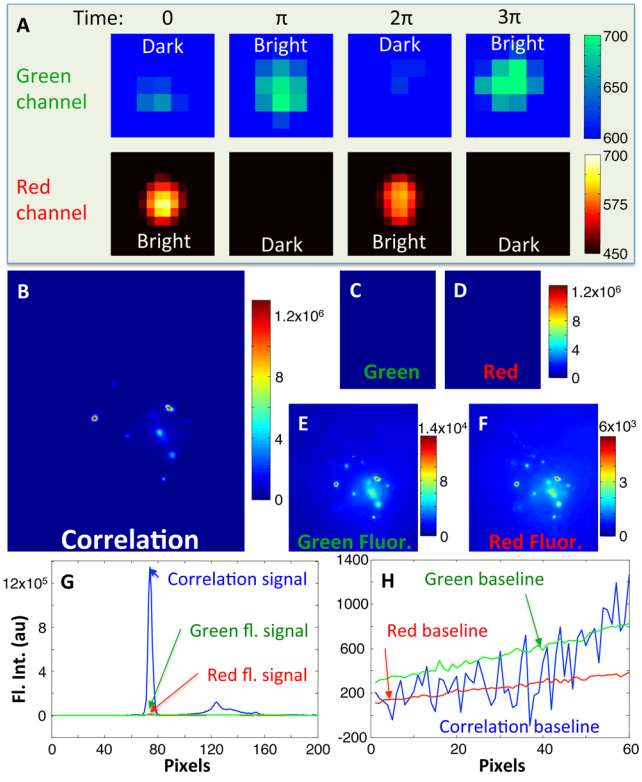

Figure 3. (A) A single PNP in a live cell undergoes red−green fluorescence photoswitching with each half-cycle or π. (B−F) The AD correlation image (B) shows a significantly boosted S/N ratio to an intensity scale at which both the red (C) and green (D) channels appear blank. At autoscale, both the green (E) and red (F) channels show patterns similar to the correlation image but with considerable noise, as evidenced by the blue color contours. (G, H) The correlation signal is orders-of-magnitude more intense than the integrated red or green fluorescence signal (G), while the correlation noise is just about a factor of 2 larger (H), thus yielding strong gain in the S/N ratio.

correlation in living cells under the pulse sequence of alternating switching lasers and the imaging laser (see the SI). The AD correlation image in Figure 3B displays a large magnitude of the correlated signals. At the same scale bar, neither the green channel (Figure 3C) nor the red channel (Figure 3D) shows a discernible signal. At autoscale, the time-integrated intensities in the green channel (Figure 3E) and the red channel (Figure 3F) appear with considerable noise and significant interfering signals. These results demonstrate that AD correlation microscopy has the ability to amplify the signals because of their unique antiphase relationship.

For comparison purposes,[7] it is instructive to quantitatively gauge the enhancement obtained by AD correlation microscopy. Figure 3G depicts the correlated signal, integrated green fluorescence intensity, and integrated red fluorescence intensity. Correspondingly, Figure 3H displays their noises in the nearby baselines. The S/N ratio in AD correlation imaging is 4384, whereas the S/N ratios for green and red fluorescence imaging are only 92 and 72. Thus, the AD correlation imaging has enhanced the S/N ratio 48 times over the integrated green fluorescence intensity and 61 times over the integrated red fluorescence intensity. Similar results were obtained from other AD nanoparticles as well as in other cells; the overall enhancement factors are 63−92 (Figures S2−S6). Therefore, molecules that undergo AD photoswitching have dramatically improved image contrast and sharpness.

Why does imaging in live cells (Figure 3) produce superior S/N ratios compared with those for imaging of nanoparticles on coverslips (Figure 2)? The reasons are that coverslips have low noise. Living cells, however, introduce systematic noise, including cell autofluorescence, light scattering caused by cellular structures, and cell inhomogeneity or topology. These factors are detrimental to the sensitivity of fluorescence imaging because conventional time-integration averaging cannot eliminate them at all. Here, AD technology, which explores the unique linkage between a reactant and its product, offers not only strong gains in signal strength and reliability but also elimination of interferences from nonswitching fluorophores and various noise sources stated above.

Nanoparticle locations in live cells were identified using AD correlation imaging and overlaid with the cell nucleus image (Figure 4). Typically, these nanoparticles were endocytosed at the cellular membrane and then transported to the perinuclear areas. However, an interesting fact revealed by Figure 4 is that a few nanoparticles lined up with a cellular protein assembly that

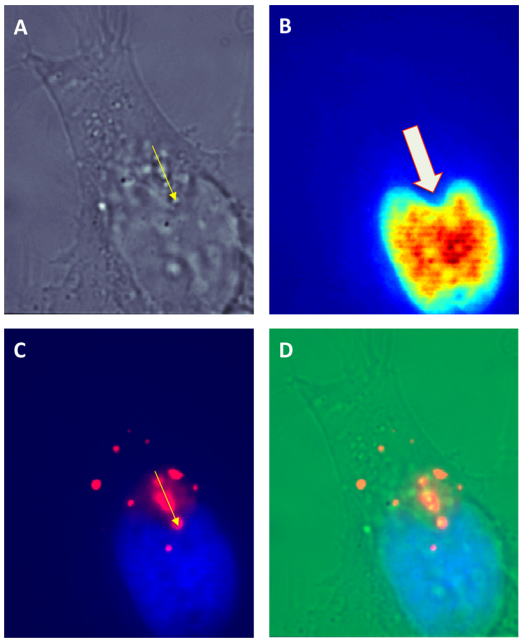

Figure 4. A living cell treated with AD PNPs was imaged under white light (A); its nucleus was confirmed with DAPI (B). The overlay of the DAPI and correlation images (C) along with the cell image (D) reveals that PNPs were associated with a protein assembly that had caused a dent in the nucleus (arrows in A−C).

DOI: 10.1021/jacs.5b01007
J. Am. Chem. Soc. 2015, 137, 4312−4315

was pressing against the nucleus envelope and had created a dent on the nucleus.

AD correlation imaging is completely different from dual-color fluorescence cross-correlation spectroscopy (FCCS).[1c,8] Dual-color FCCS provides information to calculate equilibrium or rate constants, whereas AD correlation imaging seeks to amplify the sensitivity and reliability of detection. The AD fluorescence has a distinct antiphase and thus is different from fluorescence energy transfer and others[1d,5b,9] as well as the use of two dyes[1e,10] or fluorescent proteins.[11]

In summary, AD correlation imaging thrives under adverse conditions against a strong fluorescence background or interfering matrix. Because the chemistry-enabled correlation is unique, AD imaging is exceptionally sensitive against those others that do not have this reaction-linked correlation, and thus, it is expected to have future applications in various complex systems, including solution measurements, live-cell imaging, and tissue/organ imaging.

■ ASSOCIATED CONTENT

Ⓢ Supporting Information

Methods, analyses, and additional data. This material is available free of charge via the Internet at http://pubs.acs.org.

■ AUTHOR INFORMATION

Corresponding Authors

*dequan@wsu.edu

*zytian@ucas.ac.cn

Notes

The authors declare no competing financial interest.

■ ACKNOWLEDGMENTS

This work was supported in part by the National Science Foundation (CHE-1213358). Z.T. thanks the NNSFC (Grant 21373218) and the "Hundred-Talent Program" of CAS.

■ REFERENCES

(1) (a) Nikic, I.; Plass, T.; Schraidt, O.; Szymanski, J.; Briggs, J. A. G.; Schultz, C.; Lemke, E. A. *Angew. Chem., Int. Ed.* **2014**, *53*, 2245. (b) Li, H. T.; Ying, L. M.; Green, J. J.; Balasubramanian, S.; Klenerman, D. *Anal. Chem.* **2003**, *75*, 1664. (c) Kogure, T.; Karasawa, S.; Araki, T.; Saito, K.; Kinjo, M.; Miyawaki, A. *Nat. Biotechnol.* **2006**, *24*, 577. (d) Bates, M.; Blosser, T. R.; Zhuang, X. W. *Phys. Rev. Lett.* **2005**, *94*, No. 108101. (e) van de Linde, S.; Kasper, R.; Heilemann, M.; Sauer, M. *Appl. Phys. B: Lasers Opt.* **2008**, *93*, 725. (f) Bacia, K.; Schwille, P. *Nat. Protoc.* **2007**, *2*, 2842. (g) Chen, A.; Eberle, M. M.; Lunt, E. J.; Liu, S.; Leake, K.; Rudenko, M. I.; Hawkins, A. R.; Schmidt, H. *Lab Chip* **2011**, *11*, 1502.

(2) (a) Zhu, M. Q.; Zhu, L. Y.; Han, J. J.; Wu, W. W.; Hurst, J. K.; Li, A. D. Q. *J. Am. Chem. Soc.* **2006**, *128*, 4303. (b) Irie, M.; Fukaminato, T.; Sasaki, T.; Tamai, N.; Kawai, T. *Nature* **2002**, *420*, 759.

(3) Zhu, M. Q.; Zhang, G. F.; Li, C.; Aldred, M. P.; Chang, E.; Drezek, R. A.; Li, A. D. Q. *J. Am. Chem. Soc.* **2011**, *133*, 365.

(4) Hu, D. H.; Tian, Z. Y.; Wu, W. W.; Wan, W.; Li, A. D. Q. *J. Am. Chem. Soc.* **2008**, *130*, 15279.

(5) (a) Lohani, C. R.; Kim, J. M.; Chung, S. Y.; Yoon, J.; Lee, K. H. *Analyst* **2010**, *135*, 2079. (b) Heilemann, M.; Margeat, E.; Kasper, R.; Sauer, M.; Tinnefeld, P. *J. Am. Chem. Soc.* **2005**, *127*, 3801.

(6) (a) Tian, Z. Y.; Wu, W. W.; Wan, W.; Li, A. D. Q. *J. Am. Chem. Soc.* **2009**, *131*, 4245. (b) Tian, Z. Y.; Wu, W. W.; Wan, W.; Li, A. D. Q. *J. Am. Chem. Soc.* **2011**, *133*, 16092.

(7) Li, A. D. Q.; Zhan, C. L.; Hu, D. H.; Wan, W.; Yao, J. N. *J. Am. Chem. Soc.* **2011**, *133*, 7628.

(8) (a) Kim, H. J.; Han, J. H.; Kim, M. K.; Lim, C. S.; Kim, H. M.; Cho, B. R. *Angew. Chem., Int. Ed.* **2010**, *49*, 6786. (b) Lee, N. S.; Rohan, J. G.; Zitting, M.; Kamath, S.; Weitz, A.; Sipos, A.; Salvaterra, P. M.; Hasegawa, K.; Pera, M.; Chow, R. H. *PLoS One* **2012**, *7*, No. e35521.

(9) (a) Chen, O.; Shelby, D. E.; Yang, Y. A.; Zhuang, J. Q.; Wang, T.; Niu, C. G.; Omenetto, N.; Cao, Y. C. *Angew. Chem., Int. Ed.* **2010**, *49*, 10132. (b) Deng, Z. T.; Tong, L.; Flores, M.; Lin, S.; Cheng, J. X.; Yan, H.; Liu, Y. *J. Am. Chem. Soc.* **2011**, *133*, 5389. (c) Diaz, S. A.; Giordano, L.; Jovin, T. M.; Jares-Erijman, E. A. *Nano Lett.* **2012**, *12*, 3537. (d) Diaz, S. A.; Giordano, L.; Azcarate, J. C.; Jovin, T. M.; Jares-Erijman, E. A. *J. Am. Chem. Soc.* **2013**, *135*, 3208. (e) Algar, W. R.; Wegner, D.; Huston, A. L.; Blanco-Canosa, J. B.; Stewart, M. H.; Armstrong, A.; Dawson, P. E.; Hildebrandt, N.; Medintz, I. L. *J. Am. Chem. Soc.* **2012**, *134*, 1876. (f) Zhu, L. Y.; Zhu, M. Q.; Hurst, J. K.; Li, A. D. Q. *J. Am. Chem. Soc.* **2005**, *127*, 8968. (g) Hsiang, J. C.; Jablonski, A. E.; Dickson, R. M. *Acc. Chem. Res.* **2015**, *47*, 1545.

(10) Zhu, L. Y.; Wu, W. W.; Zhu, M. Q.; Han, J. J.; Hurst, J. K.; Li, A. D. Q. *J. Am. Chem. Soc.* **2007**, *129*, 3524.

(11) (a) Wiedenmann, J.; Ivanchenko, S.; Oswald, F.; Schmitt, F.; Rocker, C.; Salih, A.; Spindler, K. D.; Nienhaus, G. U. *Proc. Natl. Acad. Sci. U.S.A.* **2004**, *101*, 15905. (b) Shroff, H.; Galbraith, C. G.; Galbraith, J. A.; White, H.; Gillette, J.; Olenych, S.; Davidson, M. W.; Betzig, E. *Proc. Natl. Acad. Sci. U.S.A.* **2007**, *104*, 20308. (c) Jathoul, A. P.; Grounds, H.; Anderson, J. C.; Pule, M. A. *Angew. Chem., Int. Ed.* **2014**, *53*, 13059. (d) Jablonski, A. E.; Vegh, R. B.; Hsiang, J. C.; Bommarius, B.; Chen, Y. C.; Solntsev, K. M.; Bommarius, A. S.; Tolbert, L. M.; Dickson, R. M. *J. Am. Chem. Soc.* **2013**, *135*, 16410.

DOI: 10.1021/jacs.5b01007
J. Am. Chem. Soc. 2015, 137, 4312−4315